ARTICLE

Downhill progressive landslides in long natural slopes: triggering agents and landslide phases modeled with a finite difference method

Stig Bernander, Anders Kullingsjö, Anders S. Gylland, Per-Evert Bengtsson, Sven Knutsson, Roland Pusch, Jan Olofsson, and Lennart Elfgren

Abstract: A large landslide in Tuve (Gothenburg, Sweden, 1977) initiated the development of a model for slope stability analysis taking the deformation-softening of soft sensitive clays into consideration. The model studies triggering agents and five phases in progressive slope failure are identified: (1) in situ, (2) disturbance, (3) unstable "dynamic", (4) transitory (or permanent) equilibrium, and (5) "global" failure. The clay resistance in these phases may differ widely; mostly due to different rates of loading. Two time-dependent failure criteria are defined: (*i*) the triggering load condition in the disturbance phase 2 and (*ii*) the transitory equilibrium in phase 4, indicating whether minor downhill displacements or a veritable landslide catastrophe will occur. The analysis explains why downhill landslides tend to spread over vast areas of almost horizontal ground further downslope. The model has been applied to landslides in Scandinavia and Canada. Three case studies are briefly discussed. The model is a finite difference approach, where local downhill deformations caused by normal forces is maintained compatible with deviatory shear deformations above — and, if relevant, below — the potential (or the established) failure surface. Software and an easy-to-use spreadsheet are introduced as well as recent developments.

Key words: landslides in long natural slopes, progressive failure in different phases, triggering agents, effects of time and rate of loading, two main failure criteria, invalidity of one singular static load condition, massive spread over level ground, finite difference method of analysis.

Résumé : Un grand glissement de terrain en Tuve (Gothenburg, Suède, 1977) a abouti à l'initiation de l'élaboration d'un modèle pour l'analyse de la stabilité des pentes en prenant la déformation-adoucissement des argiles sensibles souples en considération. Le modèle étudie les agents déclencheurs et cinq phases dans l'échec progressif de pentes sont identifiées : (1) in situ, (2) la perturbation, (3) instable « dynamique », (4) l'équilibre transitoire (ou permanent), et (5) l'échec « global ». La résistance de l'argile dans ces phases peut varier largement; principalement en raison de différents taux de chargement. Deux critères de défaillance en fonction du temps sont définis : (*i*) l'état de charge de déclenchement dans la perturbation de la phase 2, et (*ii*) l'équilibre transitoire à la phase 4, indiquant si les déplacements en descente mineurs ou un glissement de terrain catastrophe véritable se produira. L'analyse explique pourquoi les glissements de terrain en descente ont tendance à se répandre sur de vastes étendues de sol presque horizontal plus bas dans la pente. Le modèle a été appliqué à des glissements de terrain en Scandinavie et au Canada. Trois études de cas sont brièvement discutées. Le modèle est une approche des différences finies, où les déformations en descente locales causées par les forces normales sont maintenues compatibles avec les déformations de cisaillement déviant au-dessus — et si s'est applicable aussi au-dessous — de la surface de rupture potentielle (ou établie). Le logiciel et une feuille de calcul facile à utiliser sont introduits ainsi que des développements récents. [Traduit par la Rédaction]

Mots-clés : glissements de terrain dans les pentes naturelles longues, l'échec progressif dans les différentes phases, agents déclencheurs, effets de temps et le taux de chargement, deux principaux critères d'échec, invalidité d'une condition de charge statique singulière, propagation massive sur un terrain de niveau, analyse par méthode de différences finies.

Introduction

Disastrous landslides occur time and time again in long slopes of deformation-softening clays in Canada, Scandinavia, and other areas with glacial and post glacial sediments emerging from regressing seas after the glacial period. In these areas, the clay may be extremely sensitive and thus liquefy when remoulded (quick clays). In consolidated undrained triaxial tests and direct shear tests, the clays exhibit a peak strength after which the soil structure collapses leading to increased pore-water pressure and a corresponding reduction in effective stress. Liquefaction may also result from stress–strain reversals.

S. Bernander, S. Knutsson, R. Pusch, and L. Elfgren. Department of Civil, Environmental and Natural Resources Engineering, Luleå University of Technology, SE-97187 Luleå, Sweden.
A. Kullingsjö. Skanska Sweden, Johan på Gårdas gata 5, SE-405 18 Göteborg, Sweden; Chalmers University of Technology, GeoEngineering, SE-412 96 Göteborg, Sweden.
A.S. Gylland. Multiconsult, Sluppen 15, NO-7037 Trondheim, Norway; Norwegian University of Science and Technology, Geotechnical Engineering, NTNU, NO-7491 Trondheim, Norway.
P.-E. Bengtsson. Swedish Geotechnical Institute, Olaus Magnus väg 35, SE-581 93 Linköping, Sweden.
J. Olofsson. Skanska Sweden, Johan på Gårdas gata 5, SE-405 18 Göteborg, Sweden.
Corresponding author: Lennart Elfgren (email: lennart.elfgren@ltu.se).

Many slides have until the last years mostly not been explained satisfactorily by post-slide investigations when applying the classic limit equilibrium method based on perfectly plastic clay response. Instead, a strain- or deformation-softening approach is required. The development of a method based on such conditions will be discussed here.

Factors triggering landslides are often related to construction work or river erosion. In sensitive clays, a minor instability can progress (downwards) or retrogress (upwards) depending on where the instability is triggered. In both cases, massive volumes of clay may finally be involved.

Early aspects on various types of progressive failure, mostly in highly overconsolidated clays, have among other been treated by Terzaghi and Peck (1948), Kjellman (1955), Skempton (1964), Bjerrum (1967), Christian and Whitman (1969), Bishop (1971), Flodin and Broms (1981), Chen et al. (1997), and Leroueil (2001). The first author of this paper began studying the effects of highly strain-softening soils after the landslide at Tuve in Göteborg that occurred in 1977 (Bernander 1978). He has later published conference papers and reports on downhill progressive slope failures (Bernander 1985, 2000, 2008, 2011; Bernander and Olofsson 1981; Bernander and Gustås 1984; Bernander et al. 1985, 1989).

Today, progressive and retrogressive landslide failure has become a recognized phenomenon in highly deformation-softening soils. Research and development in this discipline of soil mechanics is now going on in several countries, notably in Australia, Canada, Italy, Norway, Sweden, and Switzerland. State of the art reviews and recent progress are reported in theses by Troncone (2005), Locat (2007, 2012), Thakur (2007), Quinn (2009), Saurer (2009), and Gylland (2012). Their work is also further developed in the workshop proceedings (L'Heureux et al. 2013), in papers by, e.g., Locat et al. (2008, 2011, 2013, 2015), Gylland et al. (2014), Bonadies et al. (2014), Zhang et al. (2015), and in the editorial by Puzrin (2016). Focus is often on material properties and on numerical solutions of various kinds, e.g., finite element methods.

The current paper discusses how landslides in long slopes of deformation-softening clay can be modelled as a downhill progressive failure using a finite difference two-dimensional model. The description of the initial phases of a slide is similar to what is presented in many of the recent papers referred to above. But beyond this, the following cardinal issues are in focus:

1. How do we explain the fact that extensive landslides can be triggered by relatively insignificant "local additional load effects"?
2. Is it, in the analysis, mandatory to consider the deformations in the "entire highly sheared zone" or is it merely sufficient to study those in a narrow shear band?
3. Is it important to identify distinctly "different phases" in progressive landslides? How does time affect the triggering loading conditions and further slide development?
4. Can landslide hazard in sensitive clays be correctly predicted by only one "singular failure criterion" based on static loading such as e.g., the plastic limit equilibrium failure condition?
5. Is it essential to differentiate between deformations in the zones of "unfractured clay" and corresponding conditions subsequent to the formation of a "failure surface" or shear band?
6. How do we, in these landslides, explain the massive heave and plasticization over extensive areas of gently sloping or horizontal ground?

Exemplification of the analysis of initial phases of a downhill progressive landslide

To illustrate the characteristics of a progressive failure, a simplified example is presented in Figs. 1–3. Figure 1 represents a typical stress–strain relationship for clay with strain-softening behavior. The curve can be described by the following set of parameters. The linear elastic limit is defined by the coordinates τ_{el}/γ_{el}

Fig. 1. Stress–strain (τ/γ) and stress–deformation (τ/δ) relationships in the studied example. Stage I is the condition before τ reaches $\tau_{max} = s$ and stage II is the subsequent deformation softening part.
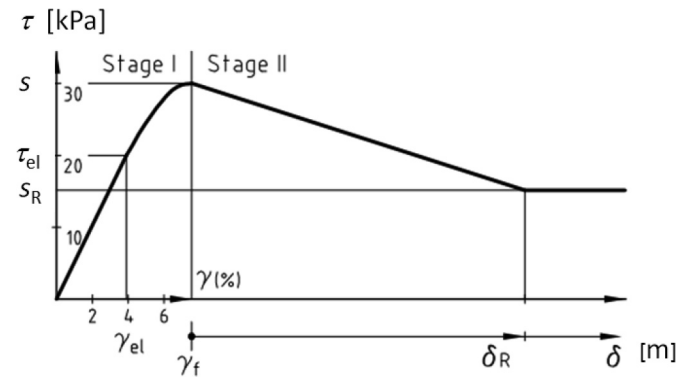
and the peak resistance by s/γ_f. Beyond the peak stress, $\tau_{max} = s$, the resistance in the failure surface is taken to be related to the slip δ in this plane. This also defines the change from stage I (increasing stresses) to stage II (softening). The deformation δ_R defines a condition when the abating shear resistance along the slip plane attains an ultimate value s_R. The values of the parameters may vary with depth and time and will be discussed later. The values given in Fig. 1 will be used in the following introductory example, adapted from Bernander (2011).

Figure 2 shows a slope, where a long portion has constant inclination β and invariable depth H to the potential failure surface. This simplistic geometry is just chosen to facilitate the understanding of the main issues involved. Yet, the current finite difference method (FDM) can deal with arbitrary geometry and varying soil strength characteristics.

Figures 2 and 3 illustrate the effects of a triggering load N_q, which in the current case is caused by an uphill load q. The top part of Fig. 2 illustrates the geometry, the middle part illustrates the shear stress, τ, and the bottom part illustrates the additional earth pressure N above the potential (or the developing) failure plane. The coordinate L (downwards) has the value $L = 0$ where the load N_q is entered. The coordinate x (in the opposite direction of L) has the value $x = 0$ at the location, where the effects of the load N_q are practically zero. This is the location where the additional earth pressure N_x, the displacement δ_x and the resulting shear stress $\tau_{x,z}-\tau_o$ are negligible. Here $\tau_{x,z}$ is the shear stress as a function of the coordinates x and z and τ_o is the in situ shear stress (which also may vary with x and z). In the example the in situ stress τ_o relates to the failure plane.

The development of the initial phases of a progressive failure is illustrated by five moments (a → e) related to gradually increasing values of the force N_q. Corresponding values are given for the shear stress τ_x (for $z = 0$) along the potential failure plane, as well as the values of the length $x = L$, signifying the distance over which the load N_q has any appreciable effect. The corresponding downhill displacement δ_x at the point of loading is given in Fig. 3, where also the first three phases of the landslide are illustrated. The total downslope earth pressure $E = E_o + N$ is introduced as the sum of the original in situ force E_o and the additional force N caused by the applied load q.

In the following the different phases will be outlined.

Significant phases of a downhill progressive landslide

Phase 1: In situ condition

In the in situ condition, i.e., "moment a" in Figs. 2 and 3, the load $N_q = N_a = 0$ and the shear stress along the potential failure

Fig. 2. Slope geometry (top); shear stresses, τ (middle); and sustained earth compression force, N (bottom); for five consecutive moments a → e illustrating the effects of increasing influential lengths L for changing upslope load, N_q. [Color online.]

Fig. 3. Displacement δ at the point of loading as a function of the load above the shear surface $E = E_o + N$ for the slope in Fig. 2. E_0 represents the in situ earth pressure. Three vital phases in the development of a landslide are indicated together with loads and displacements for the five moments a → e.

surface is τ_o. The in situ earth pressure above the potential shear surface is $E_o(x)$ and is related to the dead load of the clay and the relation between horizontal and vertical stresses. Normally "effective" stresses are considered in this phase. The deformation $\delta_a = 0$.

Phase 2: Disturbance phase

In phase 2 an additional — gradually increasing — vertical load q is applied near the top of the slope inducing an earth pressure increase corresponding to a force N_q (above the shear surface). The resulting earth pressure distribution down the slope is $E(x) = E_o(x) + N(x)$ (see Fig. 2 bottom). From now on "total" stresses usually have to be considered. Under continued loading, the peak shear resistance will be attained at the point of loading, see Fig. 2 (middle). This defines "moment b", where $\tau = \tau_{max} = s$ and $N_q = N_b$ for $x = L_b$ (Fig. 2 bottom) and the deformation is δ_b (Fig. 3).

Further increase of N_q, makes the shear stress τ_x abate due to strain-softening (Fig. 2 middle). When this stress attains the original in situ value $\tau_x = \tau_o$ at $x = L_c$ we have reached "moment c" and all available shear resistance exceeding τ_o is exploited, implying that N_q reaches its "critical" peak value $N_q = N_{crit}$ (Fig. 2 bottom and 3). This is the "first criterion" for local failure and landslide initiation. The corresponding effective influential length L_c is denoted L_{crit} and the displacement at the point of load application is $\delta = \delta_c = \delta_{crit}$ (Fig. 3) corresponding to δ_R (minus the in situ deformation due to τ_o) in Fig. 1.

Fig. 4. Critical triggering situation at the end of phase 2 (moment c in Figs. 2 and 3) with $N_q = N_{crit}$. The situation marks the transition between phase 2 and the virtually dynamic phase 3. The inelastic slip δ_{slip} develops when the shear stress τ exceeds its maximum value s thus entering the strain deformation softening stage II.
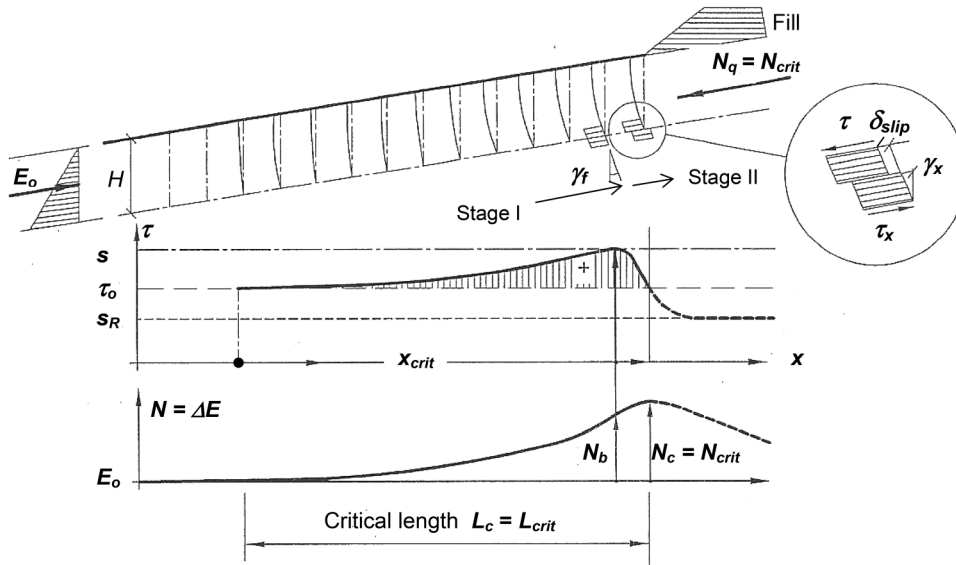

Fig. 5. Phase 4 shear stress development τ in a gentle slope ahead of an applied load $N = 0.95E_R$ (passive Rankine earth pressure). Prior to passive failure a fully developed failure zone L_P extends far beyond the foot of the slope. The maximum shear stress $1.2s$ is in the current state assumed to be 20% higher than s_{lab} obtained in laboratory tests. The deformations δ for various degrees of sensitivity s_R/s are shown in the lower figure (Bernander 2008).
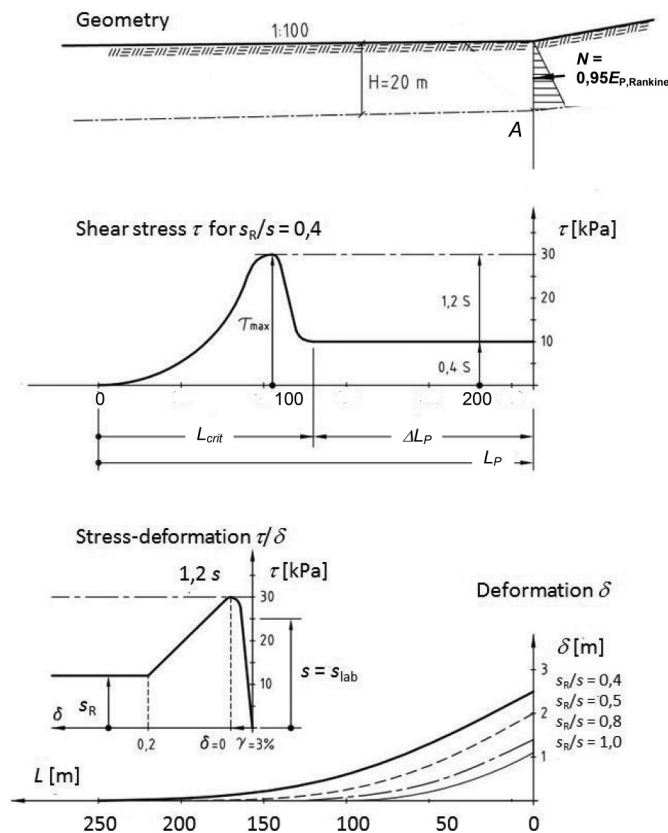
Fig. 6. Phases 4 and 5. Case 1 with a residual stress $s_{R1} = 15$ kPa represents a condition, where passive Rankine resistance just balances the forces acting downhill in phase 4, $E_P = E_o + N_1$, thus constituting the "decisive" boundary criterion for landslide incidence. Case 2 shows a phase 5 condition, with lower residual stress $s_{R2} = 10$ kPa, in which the passive earth pressure resistance E_P is exceeded. The coordinates x_1 and x_2 are the locations of the peak earth pressures $(E_o + N)_{max}$.
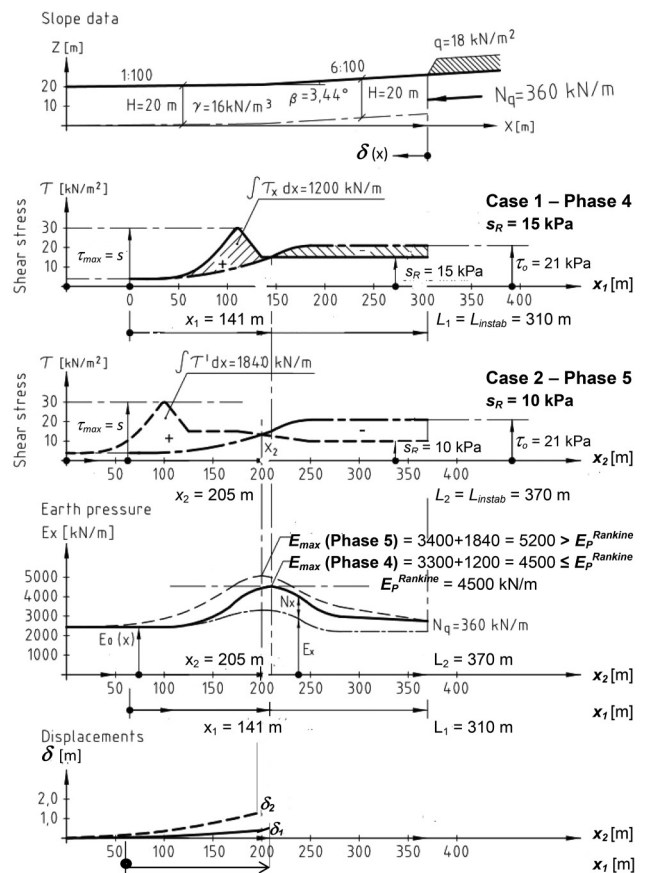
Fig. 7. Final configuration of a downhill slide. Note that there may be a zone with relative undisturbed soil between the active zone and the disintegrated passive Rankine zone, where the dynamic forces of the sliding masses are moderate (ranging between active and passive earth pressure). [Color online.]
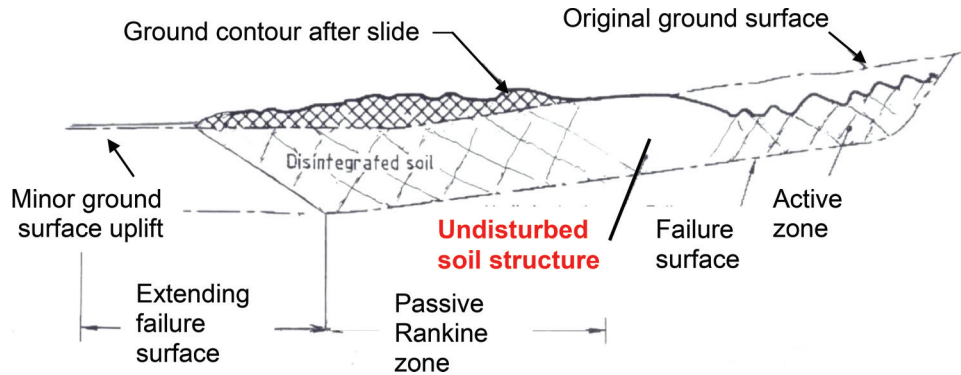
Moment c marks the end of phase 2. The possible sustained earth compression force N will now start to decrease as τ gets lower than τ_o signifying a changeover from a static situation to an unbalanced, virtually "dynamic" condition.

For a downhill progressive failure, the triggering load often consists of fills, as in Fig. 4. There also the deformation profiles along the slope are shown. A shear slip is indicated for $\tau < \tau_o$ between moments c and d in Fig. 2. The load from fills may significantly be accentuated by the effects of water saturation, explaining the fact that landslides often coincide with long spells of rain during which hydraulic pressures in the fill and in existing cracks above the ground water table may also exert pressures in downhill direction. Other common triggering load effects are rock blasting, pile driving, and vibratory activity.

Apart from inherent soil brittleness, the following factors may influence failure in phase 2:

- The slope geometry and the profile of the potential slip surface – here named "geometric brittleness";
- Nature and distribution of the applied incremental load or disturbance effect;
- Location and time span of the agents initiating failure. Rate of load application;
- Drainage conditions in the impending failure zone;
- Hydrological conditions and hydrological history.

Phase 3: Unstable "dynamic" state

When the load $N_q = N_{crit}$ is exceeded, static equilibrium is no longer possible – unless the additional loading effect is genuinely deformation-controlled and its value can be momentarily reduced, e.g., as may be the case when piling with soil-displacing elements. Otherwise, the slide now enters a virtually dynamic phase, in which "unbalanced" upslope forces are transmitted to more stable, less inclining ground further down the slope.

"Moment d" represents a condition within this dynamic phase, when the stress τ for $x = L_d$ reaches the residual shear resistance s_R (Fig. 2) and the allowable load N_q at the application point is reduced to N_d (Figs. 2 and 3).

"Moment e" represents another specific situation in phase 3, when the total passive resistance force E_P just balances the forces acting downhill. In Fig. 2 (middle) this is illustrated by the area for which $\tau \geq \tau_o$ is equal to the area for which $\tau = s_R \leq \tau_o$ (shaded). The allowable load N_q is now reduced to zero (Fig. 2 and 3). The corresponding value of L_e may be denoted L_{instab}.

From this point and on, the force N turns negative (Fig. 2 bottom) and equilibrium in phase 3 can no longer be maintained.

Phase 4: Transitory (or permanent) equilibrium

In the course of the following dynamic process, the shear resistance along the developing failure plane is effectively reduced

Fig. 8. Basic principle for the finite difference calculation is that the deviatory deformation $\Delta\delta_\tau$ due to an increase of the shear stress $\Delta\tau$ is set equal to the deformation $\Delta\delta_N$ related to the corresponding increase of the normal force ΔN. [Color online.]
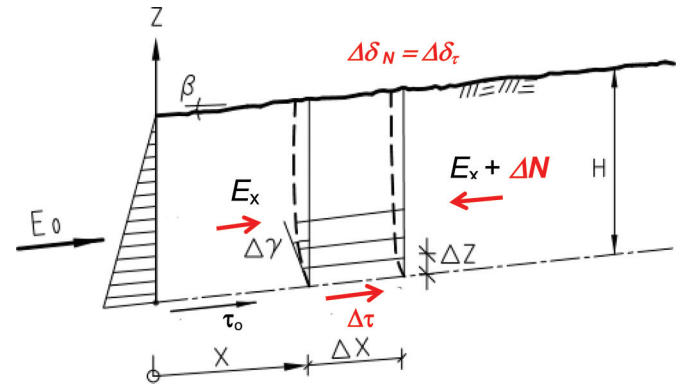
leading to massive earth pressure build-up further downslope in less sloping ground. Phase 4 represents a condition, in which the pressure build-up resulting from phase 3 is "permanently" or "temporarily" balanced by passive resistance — i.e., $(E_o + N)_{max} \leq E_P$. Phase 4 is exemplified in Fig. 5 showing a situation, where a pressure amounting to 95% of passive Rankine resistance, acts at the foot of a steep slope. The stress–deformation relationship is slightly different from the one in Fig. 1 and the short-term peak shear strength is, in this specific exemplification, assumed to be $1.2s$ during this phase (short time stress tests are known to render higher peak stress values than those obtained in normal laboratory tests).The middle figure shows the shear stress τ for a case with $s_R/s = 0.4$. The lower figure displays the resulting deformations and spreads for sensitivity ratios s_R/s varying from 1.0 to 0.4. The corresponding lengths $x = L_p = L_{crit} + \Delta L_P$ ($= L_e$ in Fig. 2), of the integral shear zones required to balance the pressure at A, range between 120 and 240 m, thus increasing as s_R/s decreases.

Provided the maximum value of E stays less than the passive earth pressure resistance E_P, the slope will merely be subjected to moderate displacements and essentially remain stable. This is not an uncommon case and the outcome may be a minor local failure or moderate displacements of a few decimetres and cracking upslope. An example of this is the slide movement in 1977 at Rävekärr, see the case study below.

Analysis of phase 4 is therefore of decisive significance, as this phase actually constitutes a measure of the potential extension of a downhill progressive landslide, and hence it's veritable degree of disaster. The ratio $E_P/(E_o + N)_{max} < 1$ in phase 4 actually constitutes the "second criterion" for landslide formation.

Fig. 9. Aerial view of the Surte landslide in the valley of the Göta River some 10 km north of the city of Gothenburg, Sweden. From north looking south. [Color online.]

Phase 5: Fully developed global failure

Yet, as already implied, the actual landslide occurs if the pressure acting downhill in phase 4 exceeds available passive resistance E_P. This condition is illustrated in Fig. 6 for a slope with changing inclination giving the initial force E_o a local maximum. In the top of the figure, the geometry of the slope is shown. In the middle of the figure, the shear stress distribution is shown for two cases. In case 1, the residual stress is $s_R = 15$ kPa and in case 2, it is lower $s_R = 10$ to 15 kPa. In the bottom of the figure, the variations of the earth pressure E and the deformations δ are shown for the two cases.

Case 1 is a situation in phase 4, where the passive resistance E_P just balances the forces acting downhill $E_o + N_1 = E_P$, thus representing the mentioned critical boundary condition for a veritable landslide event. The length of the slope from the point of no load influence to the point with maximum shear stress is $x_1 = 141$ m and the sum of the applied shear stresses is $N_1 = 1200$ kN/m giving $E_{max} = E_x + N_x = 3300 + 1200 = 4500$ kN/m "smaller or equal to" $E_{Rankine}$.

Case 2, in contrast, illustrates an ongoing failure condition in phase 5, in which static equilibrium no longer exists, i.e., $E_o + N_2 > E_P$, thus resulting in massive heave and downhill displacements. The length of the slope from the point of no load influence to the point with maximum shear stress is here longer than in case 1, $x_2 = 205$ m, due to the lower residual stress s_R and the resulting downhill forces consequently being greater, i.e., $N_2 = 1840$ kN/m giving $E_{max} = E_x + N_x = 3400 + 1840 = 5240$ kN/m "bigger than" $E_{Rankine}$, confer Fig. 6.

Phase 5 may also include the effects of dynamic inertia forces. In this phase, the slope will reach its final post-slide state of equilibrium as illustrated in Fig. 7. Due to softening of the clay along the failure surface, the resultant downslope forces increase building up an earth pressure that may cause failure in a massive passive zone of disintegrated soil. Note that the soil between this disintegrated zone and the active zone may remain relatively undisturbed except close to the failure surface.

It is here "vital" to be aware of the fact that the failure along the lengthy progressively formed failure zone with its extended shear band is — for reasons given below — of an "entirely different" nature than that of a passive failure condition in the soil mass:

1. Firstly, the two failure phenomena are not even concurrent. Already before passive downslope resistance is fully attained, both the "sheared zone" (from $z = 0$ to $z = \alpha H$) and the "established shear failure plane" (where $z = 0$), that are related to the failure in phase 3 will – provided the depth to the slip surface is sufficient – have developed far beyond the foot of the slope. This implies that before passive failure along short inclined slip surfaces has even begun to form, there already "exists" an extensive shear failure zone (including shear band), where large deformations (often in terms of metres) and substantial deformation-softening have already taken place. (cf. Figs. 5 and 7).

2. In the transitory critical stage of progressive landslide formation, earth pressures will be subject to rapid growth resulting, temporarily, in higher peak shear strengths than those corresponding to standard laboratory testing (Aas 1966; Graham et al. 1983; Bernander et al. 1985). The passive resistance is thus likely to exceed standard evaluation of passive resistance – implying that E_P for a time $t = \Delta t$ may well transiently be greater than the long term value of E_P ($t = \infty$) over the "entire" potential spread area of the landslide. This condition has been corroborated by Gylland and Jostad (2010).

3. Yet, even considering that passive failure may begin locally at the peak value of $E(x) = E_o(x) + N(x)$, the pressure distribution as defined by phase 4 will still not be affected significantly. Deformations and deformation-softening in the fully developed failure zone are "massive" in the current stage. This means that the balance between forces acting downslope and stabilizing resistance then constitutes an immense force, the "temporary" magnitude of which is practically independent of incipient

Fig. 10. Aerial photograph taken 13 days after the Surte slide (from Caldenius and Lundström 1956, © Sveriges geologiska undersökning, reprinted with permission).

heave in the soil mass. This implies in turn that developing resilience in the passive zone to be has little effect on the earth pressure distribution as defined in phase 4 or on the ensuing general failure conditions.

Points 1, 2, and 3 above explain the heave and the "enormous" spread over horizontal or gently sloping ground that is so typical of downhill progressive landslides.

Conclusion

It is thus evident that progressive landslides consist of a series of different events with mutually varying time spans, rates of loading, drainage conditions – and therefore also radically different constitutive response of the sensitive clay in the different phases of failure. Progressive landslides cannot therefore be correctly studied and predicted only on the basis of a "singular" case of "static loading".

Failure conditions

In downhill progressive landslides, there are, as indicated above, "two" decisive static failure conditions, for which the corresponding safety factors have to be defined:

1. The critical disturbing load condition at the end of phase 2, capable of triggering a landslide has a safety factor of

 $$(1) \qquad F_s^I = N_{crit}/N_q \geq 1$$

   Here N_q is the local additional load. The triggering value of the load N_q is $N_c = N_{max} = N_{crit}$ with its related values of $\delta_c = \delta_L = \delta_{crit}$ and $x_c = L_c = L_{crit}$ (see Fig. 2).

2. A "transitory" or in some cases "permanent" state of static equilibrium in phase 4 subsequent to the redistribution of earth pressures caused by the triggering load. This criterion defines the safety factor for the "global failure" condition indicating whether a veritable landslide will develop or not

   $$(2) \qquad F_s^{II} = E_p/E_{max} \geq 1$$

   Here E_{max} denotes the maximum earth pressure resulting from the virtually dynamic pressure redistribution in phase 3. In phase 4 the relationship E_P/E_{max} may be bigger or equal to 1,

Fig. 11. Plan of the Surte slide area showing elevation contours and a longitudinal section A–A of the slide. The point marked (P) on the plan is the location in the steepest portion of the slope, where piling operations were going on at the time of the slide occurrence. Section B–B marks the section being analysed in Fig. 13. [Color online.]
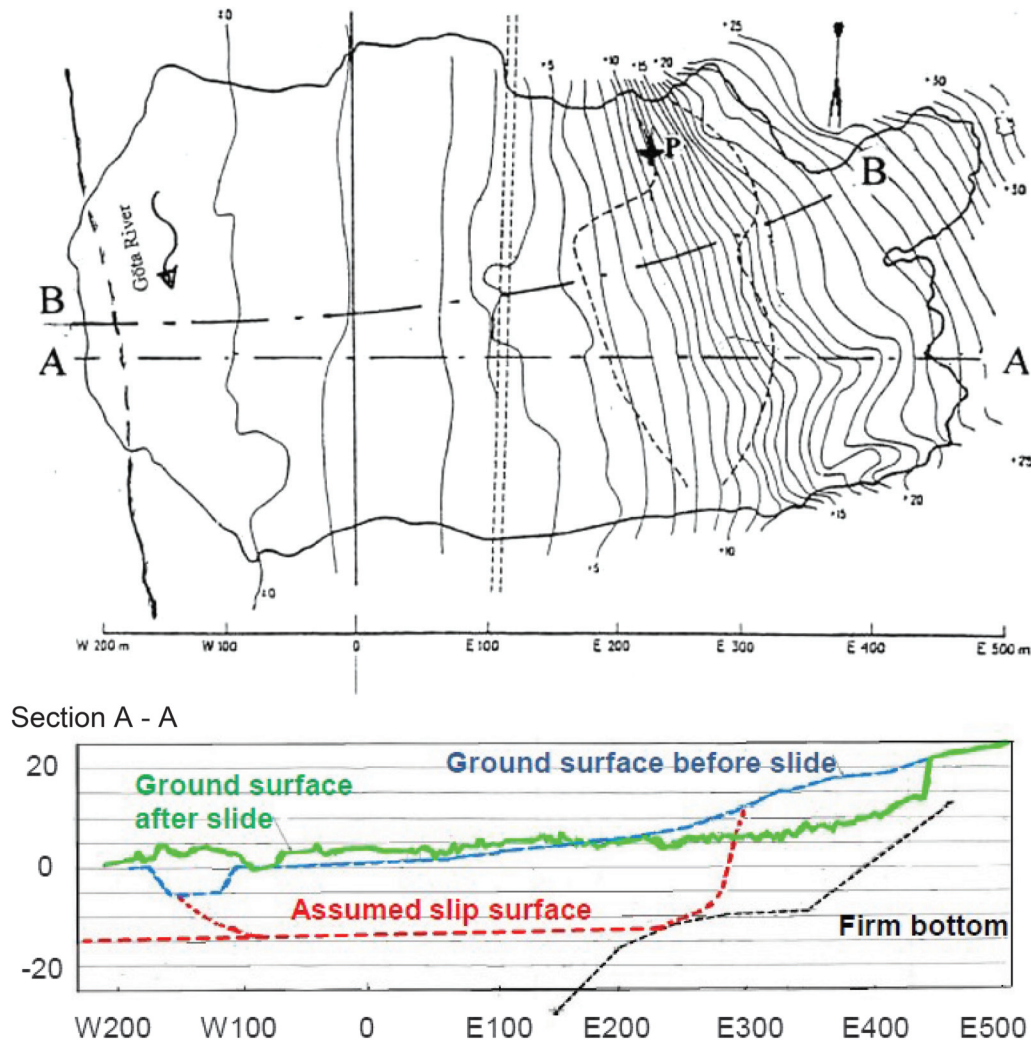
but if it turns out to be less than 1, the slide will enter phase 5 and a global failure will occur.

The two criteria were proposed by Bernander and Olofsson (1981) and Bernander et al. (1985) and in this journal by Locat et al. (2011).

Basics of the finite difference model (FDM)

The failure modes discussed above can be modeled with a FDM (Bernander 1985, 2000, 2008, 2011; Bernander and Gustås 1984; Bernander et al. 1985, 1989). The method is illustrated in Appendix A (Fig. A1) by the analysis of a long slope with variable inclination β and depth H to the firm bottom, whereas Fig. 8 shows the analysis applied to a simple case with constant inclination β and depth H. The slope is initially in equilibrium and the in situ shear stresses at the potential failure plane are τ_o. The objective of the simplified analysis is to demonstrate the effects of an additional local load upslope.

The integration process starts at a point ($x = 0$) further down the slope, where the influence of the additional load N_q is negligible, by choosing an initial shear stress increment at the potential failure plane $\Delta\tau$ at a distance $x = \Delta x$. The corresponding increase of the normal force N and the associated downhill axial displacement $\delta(N)$ may then directly be determined.

In the analysis the mean downhill deformation in each element caused by normal forces is maintained compatible with the deformation generated in the lower portion of the element by shear stresses in the potential (stage I) or the established shear failure surface (stage II). By selecting new values of $\Delta\tau$, this equation can readily be adjusted so that the compatibility criterion is satisfied, i.e.,

$$\delta_x(N) = \delta_x(\tau)$$

The process is further presented in Appendix A.

Varying geometry, different constitutive relationships, and time spans can in this context be dealt with in a computer program originally developed in 1984.

In slopes with constant inclination and depth to the slip surface, the analysis can readily be carried out in an easy-to-use spreadsheet (Excel). A simplified version of this spreadsheet is presented in Rehnström (2013).

The advantage of the FDM as outlined above relative to more advanced numerical simulations using e.g., the finite element method (Jostad et al. 2013), the material point method (Zabala and Alonso 2011) or X-FEM (Thakur and Septanika 2008) is that one avoids all issues of numerical instability, nonuniqueness of the solution, strain localization, regularization techniques, and inter-

Fig. 12. Stress–deformation relationships for different phases of a slide: in situ (phase 1), disturbance (phase 2), and global failure (phase 4 and 5). (See also Table 1.)
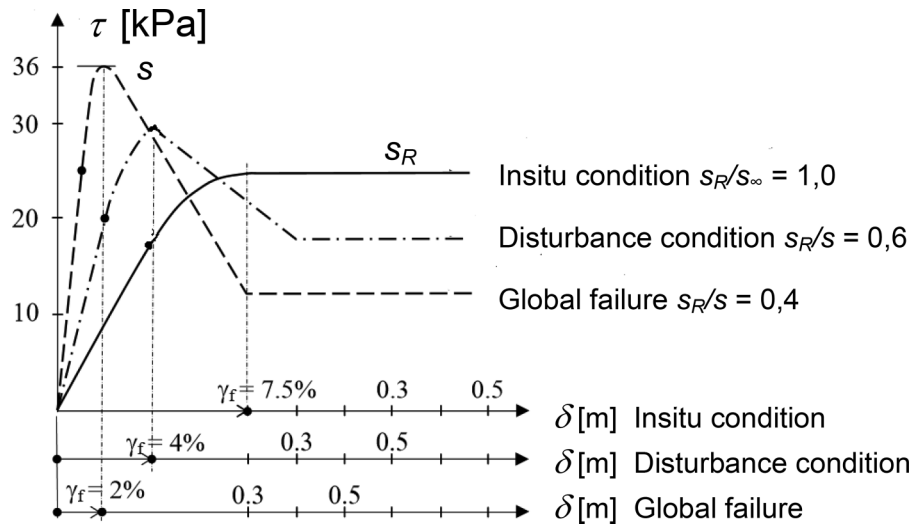

Table 1. Input parameters and results for the Surte slide.

Elastic parameters: γ_{el}, τ_{el}, G $(= \tau_{el}/\gamma_{el})$, E $(= 2(1 + \nu)G \approx 3G)$	Maximum parameters: γ_f, s, s_R/s	Loads and earth pressures: N, E, K_o $(= \sigma_h/\sigma_v)$	Lengths and deformations: L, δ
Phase 1: In situ condition			
$\gamma_{el} = 3.75\%$	$\gamma_f = 7.5\%$	$\rho g = 15.5$ kN/m³	—
$\tau_{el} = 18$ kN/m²	$s_\infty = 24$ kN/m²;* $s_R/s_\infty = 1.00$	$K_o = 0.55$ (horizontal ground)	—
$G_o = 480$ kN/m²; $E_o = 60s_\infty \approx 1440$ kN/m²; $E_{mean} = 60s_{\infty,mean}$	—	$N_o = 138$ kN/m; $E_{max} = 1673$ kN/m	$L_{N,o} = 120$ m
Phase 2: Disturbance condition			
$\gamma_{el} = 2\%$	$\gamma_f = 4.00\%$	—	—
$\tau_{el} = 20$ kN/m²	$s = 30$ kN/m²;† $s_R/s = 0.60$†	$K_o^{max} = 0.594$ (computed)	—
$G_o = 1000$ kN/m²; $E_o = 100s \approx 3000$ kN/m²; $E_{mean} = 100s_{mean}$	—	Force induced: $N_{crit} = 192$ kN/m; $E_{max} = 1665$ kN/m	$L_N = 0$ m; $L_{crit} = 114$ m; $\delta_{crit} = 0.15$ m
	—	Deformation induced: $N_{crit} = 0$ kN/m; $E_{max} = 1770$ kN/m	$L_N = 50$ m; $L_{instab} = 162$ m; $\delta_{instab} = 0.29$ m
Phase 4: Global failure condition			
$\gamma_{el} = 1\%$	$\gamma_f = 2.0\%$	—	—
$\tau_{el} = 24$ kN/m²	$s = 36$ kN/m²;‡ $s_R/s = 0.4$–0.25	K_o (computed)	—
$G_o = 2400$ kN/m²; $E_o = 200s \approx 7200$ kN/m²; $E_{mean} = 206s_{mean}$	—	$N_{max} = 3400$ kN/m; $E_{max} = 5300$ kN/m; $E_{Rankine} = 4300$ kN/m (max); $(E_R/E)_{min} \approx 0.8$	$L_{Emax} \approx 265$ m; $L_{E>E(Rankine)} \approx 310$ m

*In the current state, s_∞ signifies the long time shear resistance–drained conditions.
†Mean values applying to the initiation zone.
‡Mean value applying to the down-slope failure zone.

nal length parameters. The use and interpretation of the result is hence more transparent and available for being evaluated correctly by the user.

Case studies

Surte landslide

The Surte landslide on the bank of the Göta River some 15 km north of Gothenburg, Sweden, took place soon after 0800 on 29 September 1950. The main slide, involving some 24 ha (1 ha = 100 000 m²) of ground, swept away 31 family houses and 10 outhouse units. Due to the type of wooden family houses and the time — most residents already having gone to work elsewhere — the death toll was limited to one person.

The south-bound branch of the Göta River, which is navigable for heavy shipping transport, was blocked for 2 months. The north-bound railway and highway were displaced varying distances up to 150 m, blocking road and railway traffic for 10 and 19 days, respectively. Transportation and industry incurred serious damage.

Figures 9 and 10 are aerial photos of the slide area. Figure 11 shows a plan and a longitudinal section of the slide. The inclination in the steepest uphill part was about $5 \rightarrow 7{:}100$ and the mean value further downhill only 2:100. The quick clay properties will be discussed below. The actual slide event was observed by a number of people within and outside the slide area. One of them summed up his impressions as follows (Caldenius and Lundström 1956):

> The whole ground was moving rather slowly at a speed that can approximately be compared to that of the Bohus ferry. (Estimated speed a few metres per second.) The movement did not proceed at the same speed all the time — the speed increased progressively and the movement finally ceased when the ground piled up against the opposite side of the river. Then the ground rose and folded. However, folding had already begun during the first stage of the movement. House No. 13 toppled very slowly when the slide was approaching the opposite side of the river. Water and clay were lifted very high. Cracks of various sizes were formed during the course of the slide. At first, the ground moved straight

Fig. 13. Static earth pressure distribution in the Surte slide in phase 4 subsequent to the progressive failure phase (phase 3), but prior to the slide proper resulting in disintegration and heave in a state of passive failure (phase 5). The figure indicates that even the static forces developed in the progressive phase of the ground movement suffice to explain the passive spread of the passive zone over almost horizontal ground. [Color online.]
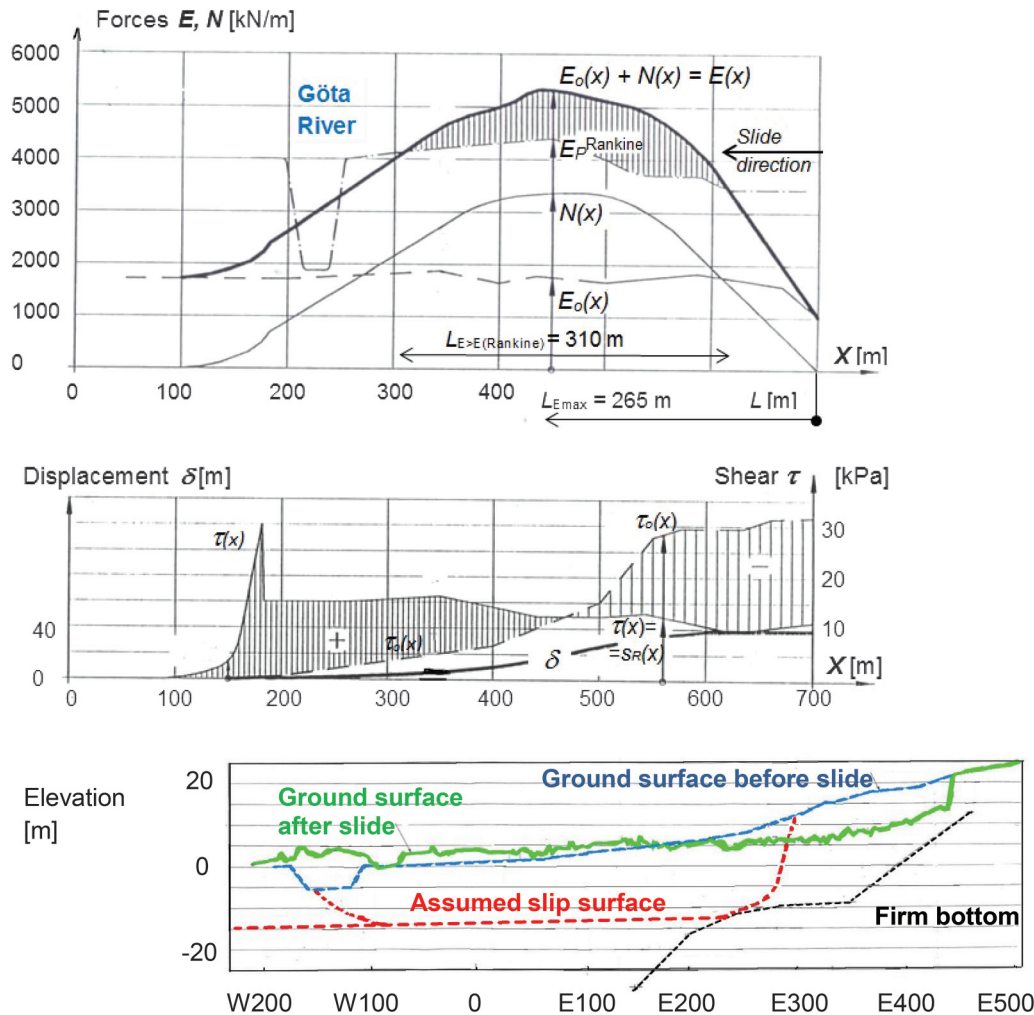
down towards the river, but further down the slide widened, while the main part of the ground continued straight ahead.

Another important witness, standing in her kitchen and facing south, told among others the following:

> She first noticed that a pile driving machine and the ground around it began to subside and that the men engaged in pile driving started to run away. Then she observed that the houses beyond were also moving. ….The pile driving machine did not topple until the last stage of the movement. A large number of cracks formed in the ground. The movement was wavelike and smooth. The houses seemed to sail along.

With reference to Figs. 1 and 12, the characteristic parameters in Table 1 have been used in this study. Different constitutive relationships are used in the different phases of the landslide and the likely stress-deformation relationships are shown for (i) the in situ condition, (ii) the disturbance condition and (iii) the global failure. In the table, $s = \tau_{max}$, denotes the peak shear strength and s_∞ is the maximum shear resistance under long term conditions. G is the elastic shear modulus and $E = 2(1 + \nu)G$ is the modulus of elasticity. Sensitivity studies show that variations of the here assumed properties do not change the outcome of the analysis in a decisive way (Bernander 2011).

In phase 1 (see Table 1), the available shear strengths in the steepest part of the slope do not match an in situ shear condition based solely on weight and slope inclination. According to the analysis, this stress difference corresponds to a force $N_o = 138$ kN/m implying that already in the in situ condition, the soil masses were to some extent balanced by elevated earth pressures in less inclined ground further down the slope (comparable to moment b in Fig. 2).

Two disturbance conditions are studied in phase 2: (i) one which is "force" induced with a critical additional load $N_{crit} = 192$ kN/m and (ii) one which is "deformation" induced with a critical value of deformation of $\delta_{instab} = 0.29$ m (corresponding to δ_e in Fig. 3). The force disturbance would correspond to a rapidly applied overload of only $q_{crit} \approx 192/18 = 10.7$ kN/m² extending 18 m upslope of point P in Fig. 11.

However, the Surte slide was probably triggered by ongoing pile driving for the foundation of a family house at the time of the slide event. The number of piles in the foundation was not quite sufficient to generate a downslope displacement of the magnitude of $\delta_{instab} = 0.29$ m, but it is very likely that the piling activities also locally induced high pore-water pressures and loss of shear strength in possible local seams of coarser moraine outwash in the clay formation. Such coarse strata commonly inter-

Fig. 14. Aerial photograph of the Tuve slide with East in the top. The slide started in the middle of the photo and moved beyond the Kville creek (top) (© Gothenburg Museum of Natural History, reprinted with permission). [Color online.]

mix with clay sediments in the vicinity of the ancient shores of the regressing post-glacial seas. A pore pressure rise of some 2 m would have been enough to initiate a failure (Bernander 2011). Significantly higher excess pore-water pressures than 2 kN/m² are often observed during piling operations.

The global failure condition illustrated in Fig. 13 represents the situation at the end of the progressive phase 3, in which unbalanced forces in the steeper parts of the slope have been transferred further downslope, resulting in massive build-up of earth pressures (phase 4) in more level ground. Calculated earth pressures E, shear stresses τ and displacements δ along the slip surface, and ground surface elevation are shown in the top, middle, and bottom parts of the figure, respectively. The length over which the passive Rankine resistance E_{Rankine} is exceeded by the resulting maximum earth pressure $E_{\max}$ is $L_{E>E(\text{Rankine})} = 310$ m.

It should be observed that the earth pressures in Fig. 13 are calculated on the assumption that the potentially sliding soil volume transiently retains its geometrical shape before possible disintegration in passive failure. This is justified because the slip surface under the valley floor is fully developed far beyond the foot of the slope already in phase 4. In Fig. 13 this distance is more than 400 m prior to the potential final breakdown of the passive zone in phase 5 and is therefore not concurrent with the final dramatic event constituting the actual landslide.

The analysis of the Surte slide highlights how a local, seemingly trivial disturbance in a vulnerable part of the slope had the potential of developing into a great disaster, massively destabilizing about 240 000 m² of ground that had remained stable for thousands of years. And yet, hypothetically, the slope may have remained stable to this day if the piling job had not taken place, or if it had been carried out in a different way.

Tuve landslide

The landslide in Tuve, a community in North Gothenburg, Sweden, took place on the 30 November 1977, just after 1600 — i.e., at a time that must have reduced the death toll significantly because people had not yet returned from work or from school. In all, the

slide resulted in nine deaths, the total destruction of 65 family houses and a drastic change of the topography of some 270 000 m² of ground. Settlements in the active zone of about 10 m and horizontal displacements up to 200 m were recorded. Upheaval in the passive zone of about 5 m over a distance of some 300 m was noted (see Figs. 14 and 15; Larsson and Jansson (1982)).

Two main phases could be identified, namely an initial slide event encompassing the ground east of line B–B in Fig. 15 and a secondary retrogressive stage covering the area west of line B–B. The initial slide is presumed to having been triggered by local instability in the steepest portions of the slope, i.e., near and upslope of the Tuve Church Road (running diagonally from SE to NW in Fig. 15).

The characteristic parameters in Table 2 have been used as input in this study. The total height of the slope is less than 20 m with an inclination in the steepest part of about 5:100 and further downhill only 2:100. The clay properties are discussed below. In phase 1, available shear strengths do not match the shear stresses in the steepest part of the slope as was the case in the Surte slide. This corresponds to a force $N_o = 671$ kN/m and implies that already in the in situ condition, the soil masses were shored up by incremental earth pressure in less inclined ground further down the slope. Because of this condition, the relationship between horizontal and vertical stresses $K_o = \sigma_h/\sigma_v$ increases from 0.55 to maximum 0.64 along the slope. It also implies that the length over which shear stresses and deformations can be induced by local load effects N_q is limited.

The vital consequence of this is that, due to the fact that the deformations related to $N_q = N_{\text{crit}}$ in this case do not materialize beyond the distance of $L_{\text{crit}} = 91.2$ m downslope of the load, passive resistance there cannot be utilized for balancing the additional local load N_{crit}, even in the state of impending progressive failure. This applies in particular to an extensive slope such as the one in Tuve, measuring at least 300 m, and where the soils were very sensitive in the upper parts. According to Table 2, the critical load N_{crit}, sufficient to initiate local failure in the steepest part of the

Fig. 15. Landslide at Tuve, 1977. Topography of the valley before the slide and boundaries of the slide area. Results of the analysis of the initial downhill slide, i.e., to the right of boundary B–B, are shown in Fig. 16 (Bernander 2011).
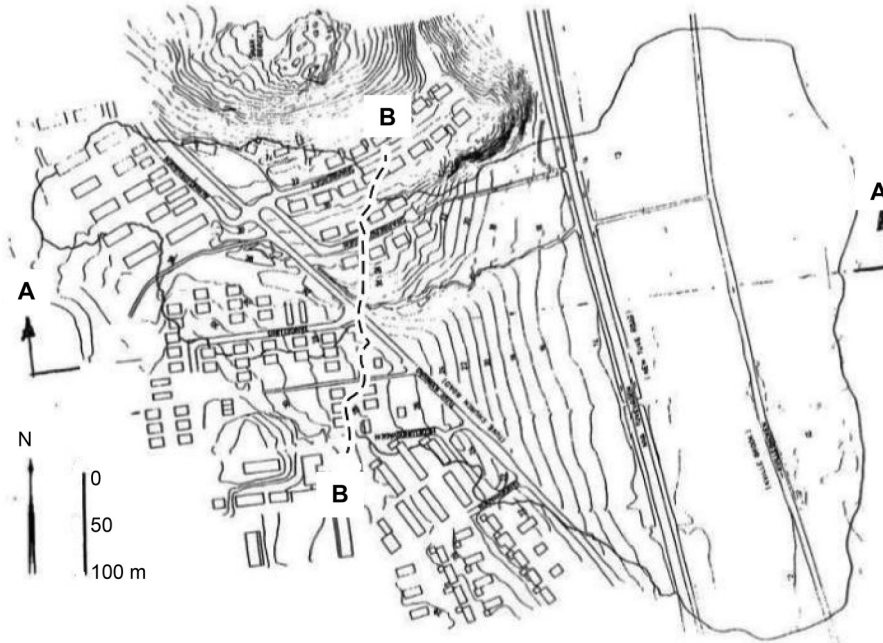

Table 2. Input parameters and results for the Tuve slide.

Elastic parameters: γ_{el}, τ_{el}, G $(= \tau_{el}/\gamma_{el})$, $E = 2(1 + \nu)G \approx 3G$	Maximum parameters: γ_f, s, s_R/s	Loads and earth pressures: N, E, K_o $(= \sigma_h/\sigma_v)$	Lengths and deformations: L, δ
Phase 1: In situ condition			
$\gamma_{el} = 2.5\%$	$\gamma_f = 7.5\%$	$\rho g = 16.5$ kN/m³	—
$\tau_{el} = 12$ kN/m²	$s_\infty = 24 \rightarrow 30$ kN/m²;* $s_R/s_\infty = 1.00$	$K_o = 0.64$	—
$G_o = 480$ kN/m²; $E_o = 60s_\infty \approx 1440$ kN/m²;	—	$N_o = 671$ kN/m; $E_o = 4169$ kN/m	$L_{N,o} = 240$ m
$\quad E_{mean} = 60s_{\infty,mean}$			
Phase 2: Disturbance condition (force induced)			
$\gamma_{el} = 2\%$	$\gamma_f = 4.67\%$	—	—
$\tau_{el} = 16.2$ kN/m²	$s = 27* \rightarrow 33^\dagger$ kN/m²; $s_R/s = 0.60$	K_o‡	—
$G_o = 810$ kN/m²; $E_o = 90s \approx 2430$ kN/m²;	—	$N_{crit} = 75.8$ kN/m; $E_{max} = 2572$ kN/m	$L_{crit} = 91.2$ m;
$\quad E_{mean} = 90s_{mean}$			$\quad \delta_{crit} = 0.055$ m
Phase 4: Global failure condition			
$\gamma_{el} = 1\%$	$\gamma_f = 2.0\%$	—	—
$\tau_{el} = 20$ kN/m²	$s = 30* \rightarrow 40^\dagger$ kN/m²; $s_R/s = 0.3–0.1$	K_o‡	—
$G_o = 2000$ kN/m²; $E_o \approx 6000$ kN/m²;	—	$N_{max} = 9128$ kN/m; $E_{max} = 15\ 035$ kN/m;	$L_{Emax} \approx 456$ m;
$\quad E_{mean} = 200s_{u,mean}$		$\quad E_{Rankine} = 12\ 852$ kN/m (varies);	$\quad L_{E>E(Rankine)} \approx 450$ m
		$\quad (E_R/E)_{min} = 0.84$	

*Mean values applying to the initiation zone.
†Mean values applying to the down-slope failure zone.
‡As computed in the in situ condition.

slope, only amounts to 75.8 kN/m. Assuming fully undrained conditions in the disturbance phase the value of N_{crit} merely corresponds to a distributed load on the ground surface q_{crit} of about $75.8/17 \approx 4.5$ kN/m² (with a premised extension of the load of 17 m).

As in the Surte case study, variations of the parameters do not change the outcome of the analysis in a decisive way (Bernander 2011).

Figure 16 displays the calculated earth pressure distribution (top), shear stresses (middle), slope geometry and location of the slip surface (bottom). The figure represents the situation at the end of the progressive redistribution in phase 3, i.e., at the critical transitory condition in phase 4 that is bound to develop into phase 5.

A dynamic analysis of the Tuve landslide using a schematic geometry has been performed with step by step numerical calcu-

lations in the time domain based on progressive failure development and Newton's laws of motion (Bernander and Gustås 1984). The time interval between the discrete steps in the computation was about 1 s. In Fig. 17, elevations and shear stress distributions are illustrated for three phases from a sequence of results: (*a*) phase 3, unstable "dynamic"; (*b*) phase 4, transitory equilibrium; and (*c*) phase 5, fully developed global failure. In the elevations, increasing earth pressure intensities are illustrated with shades of yellow → green → dark green → black, where black indicates that passive Rankine pressure is exceeded. In the stress diagrams, the red color indicates from right to left: increasing stresses τ, peak stress s, and the effects of deformation softening down to the residual stress s_R. The stresses marked in orange color represent the balance between the effects of downhill forces and the residual shear resistance. According to the calculations, the

Fig. 16. Tuve landslide in phase 4, along section A–A in Fig. 15: static earth pressure distribution (top), shear stresses (middle), and elevation (bottom), subsequent to the progressive failure phase, but prior to the slide proper resulting in disintegration and heave in passive failure (phase 5). A major part of the spread of the passive zone over almost horizontal ground can thus be ascribed to the static forces developed at the end of the dynamic progressive phase 3 of the ground movement (Bernander 2000).
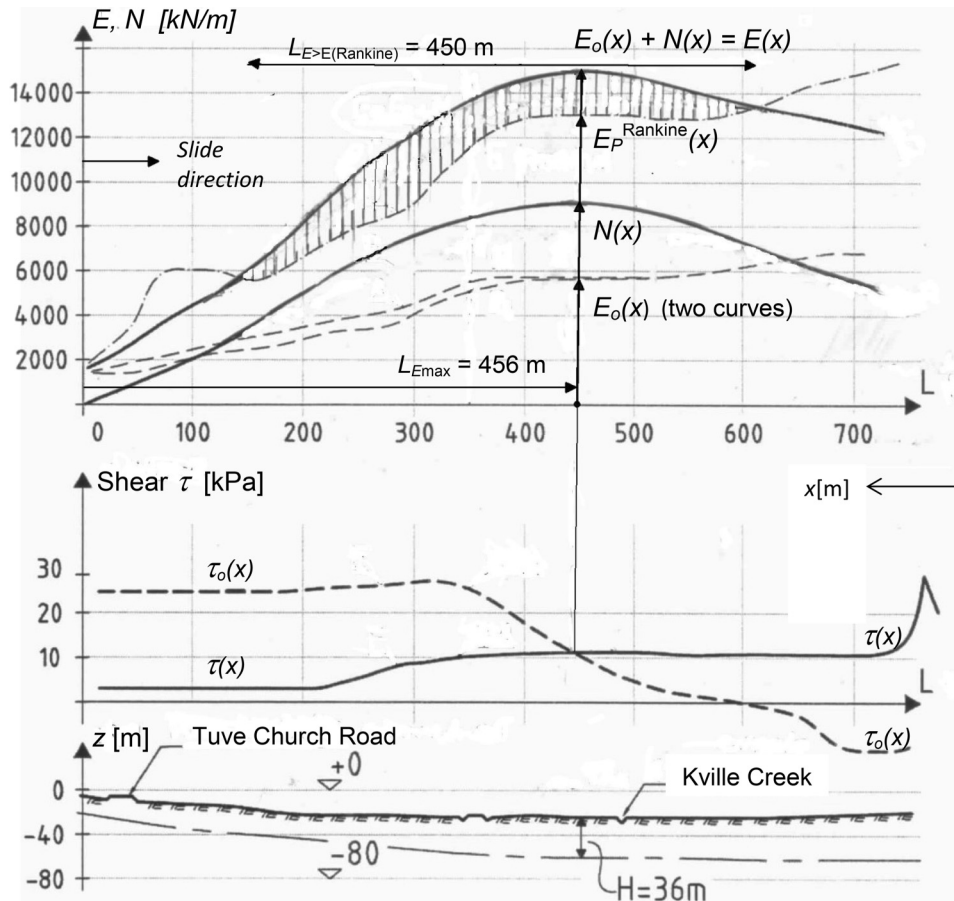
time to failure is about 22 s. However, it is conceivable that, in reality, time dependent fracture and disintegration processes prolong the different phases of the slide.

The progressive failure analysis indicates that the upper part of the slope was extremely vulnerable to additional short-term loading and unprecedented disturbance related to human activity of various kinds. The analysis also provides a logical and quantitatively consistent explanation of the vast spread of the slide over almost horizontal ground. Furthermore, the analysis also highlights the fact that landslide displacements in sensitive clay are not confined to its directly visible topographical appearance.

The causes of the Tuve slide are probably local disturbances generated by high ground water pressures due to prolonged precipitation in combination with the effects of additional load from a road embankment applied a few years before at the Tuve Church Road.

Rävekärr slide movement

The slide took place in 1971 at Rävekärr, some 8 km south of Gothenburg in the gently sloping ground of a side valley opening out into the Mölndal River valley. Figure 18 shows a plan and a representative section of the 550 m wide slide area. The valley consists of soft normally consolidated very sensitive clay that below the dry crust has a strength of about $s = (10–15 + \gamma z)$ kN/m². The inclination at the crack where the slide movement started was about 5:100 and decreased further down the valley.

A minor piling project for a family house had been started. When the sixth pile was being driven a crack in the ground sud-
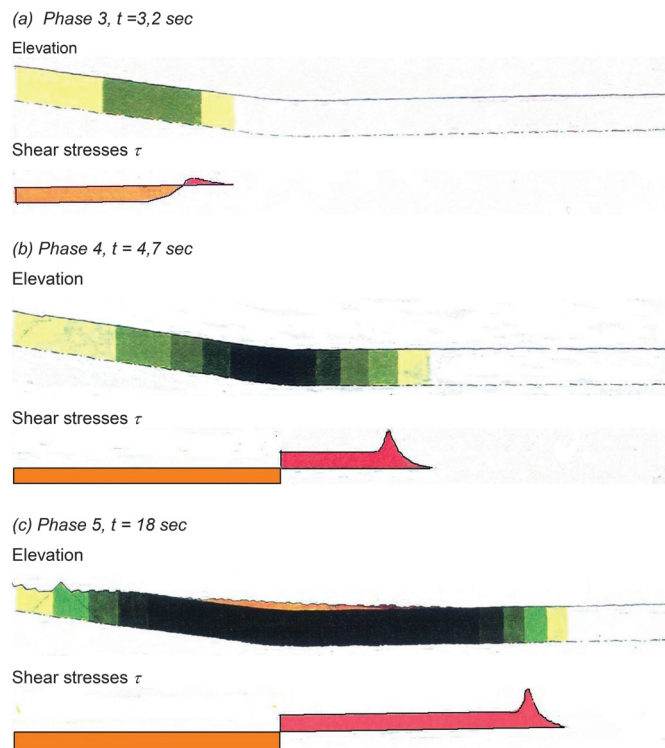
denly appeared. The crack propagated at a speed judged by an eyewitness to be about the pace of a running person ($\approx$5 m/s). It halted some 130 m northwards against an outcrop of firm ground. In the opposite direction, the crack in the ground passed through an area of family housing following the contour lines of the slope and came to a stop some 420 m from where it had started (Löfquist 1973).

The final width of the crack and the related vertical offset due to local active failure was only 0.2 to 0.3 m. The total area, subject to documented downslope displacement in this order of magnitude, was about 150 000 m². Slip surfaces were documented at depths of 5–7 m in the upper part of the slide and angular deformations were recorded at 13 and 33 m depth in the lower parts of the valley.

Although the ground downslope of the crack was somewhat displaced, no passive zone with measurable heave was observed, implying that the crack originated from deformations related to the redistribution of stresses and earth pressures in accordance with the dynamic phase (phase 3) of a progressive failure. Before the slide event, elevated ground upslope had essentially been stabilized by the in situ shear forces. The redistribution in phase 3 meant that the upslope loss of shear strength was compensated by a corresponding build-up of earth pressures in the downslope area. Hence, the documented displacements forming the slide relate to this transfer of forces of a virtually dynamic nature.

The slide at Rävekärr represents a case, where the earth pressure increase in the "post progressive" state of equilibrium (phase 4)

Fig. 17. Dynamic analysis illustrating elevations and shear stresses at different times from the initiation of a slide in the upper left part of the figure: (*a*) phase 3, (*b*) phase 4, and (*c*) phase 5. In the elevations, increasing earth pressure intensities are illustrated with shades of yellow → green → dark green → black, where black indicates that passive Rankine pressure is exceeded. In the shear stress diagrams, the red color indicates from right to left: increasing stresses, peak stress *s*, and softening reaching the residual stress s_R; the orange color indicates the difference between shear stresses due to forces acting downhill and the resistance s_R (Bernander and Gustås 1984: Bernander 2000, 2011). [Color online.]

(a) Phase 3, t = 3,2 sec

(b) Phase 4, t = 4,7 sec

(c) Phase 5, t = 18 sec

Fig. 18. Plan and section through the slide area at Rävekärr. Observe the gentle slope gradient. Slip surfaces were documented at depths of 5–7 m in the upper part of the slide and angular deformations were recorded at 13 and 33 m depth in the lower parts of the valley (modified from Löfquist 1973). [Color online.]

remained smaller than the passive resistance at the foot of the slope. This specific condition, i.e., $(E_o + N)_{max} < E_P$, was manifestly confirmed by routine progressive failure analysis.

The slide movement at Rävekärr indicates that the time range for progressive failure of this type to take place can be a matter of tens of seconds or a few minutes.

It may be concluded that the ground movement at Rävekärr can be classified as an "unfinished landslide" where, owing to the low slope gradient, the depth of the soil in the triggering location and (or) to moderate sensitivity of the soil further downslope, the progressive failure did not terminate in massive upheaval of the passive failure zone. There are many examples of the described kind of slide movement in parts of the Swedish West Coast, although seldom being as extensive as the one in Rävekärr.

Landslide prediction: examples and comments

A vital question is the way critical portions of a slope will respond to additional loading or disturbance. The "time horizon" for a disturbance is usually expressed in terms of "days", "weeks" or "months", whereas the slope itself has existed for "hundreds or thousands of years" under diverse extreme climatic conditions. So, what is likely to ensue? Will local instability just result in minor movements and cracking in the upslope "active zone" — i.e., a lasting equilibrium in phase 2 or phase 4 – or will it terminate in a disastrous landslide (phase 5) with heave and spread over vast areas?
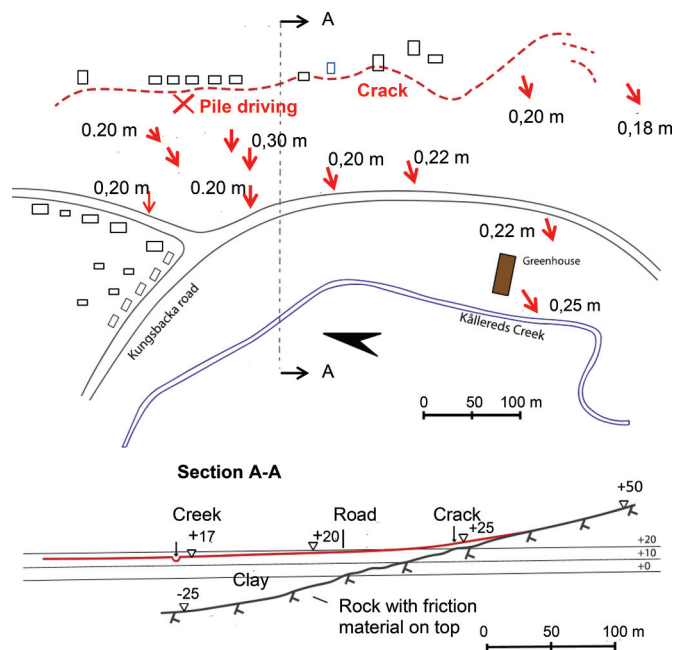
To begin with, an estimate of the in situ stress conditions has to be defined. Often the horizontal earth pressure can be estimated as $E_o \approx K_o(0.5\rho gH^2)$ with K_o being the ratio between horizontal and vertical in situ stresses along the slope ($K_o = \sigma_h/\sigma_v$). The K_o values may be chosen empirically on the basis of past experience. However, they may also be calculated on the basis of a reasonable long term stress–deformation relationship — the basic idea being that creep in a slope can be treated as an extremely slow progressive failure process. In the absence of specific tests related to creep, long-term shear strength and perfect plastic properties in the soil can be applied in this context. The input value of K_o may typically vary between 0.5 and 1.0 in different parts of the slope. Possible inaccuracies in the first assessment of the K_o values may subsequently be adjusted by repeating the analysis on the basis of the results of the foregoing assessment.

In the preliminary assessment of the stability of a slope due to a disturbing agent, there are two important issues to be considered — i.e., will the residual shear resistance s_R stay greater than the in situ stress τ_o or not? The residual shear resistance s_R can be determined by relevant testing procedure or — which is probably most reliable — by back-analysis of similar landslides applying a progressive failure mode.

In the first case, i.e., if the residual stress s_R remains greater than τ_o, the slide movement will not be progressive in the sense used in this paper. The slope will essentially remain stable even when subjected to large deformations and the load N_q will not be limited to any specific critical value in the disturbance phase.

In the second case, i.e., when the current value of s_R may fall below τ_o, the critical load N_{crit} and the critical deformation δ_{crit} have to be determined and compared with currently applied loads and deformations.

A study of the critical load for different slope conditions is summarized in Fig. 19.

The critical load in the example varies from $q_{crit} = 7$–25 kN/m² for different slope gradients and clay sensitivities s_R/s_{lab}. Note that the triggering load is relatively little affected by the degree of strain softening parameter — especially for steeper values of the slope

Fig. 19. Critical triggering load q_{crit} as function of slope inclination β and residual shear resistance s_R/s_{lab}, where s_R is the ultimate residual stress and s_{lab} is the maximum stress obtained in laboratory tests (Bernander 2008).
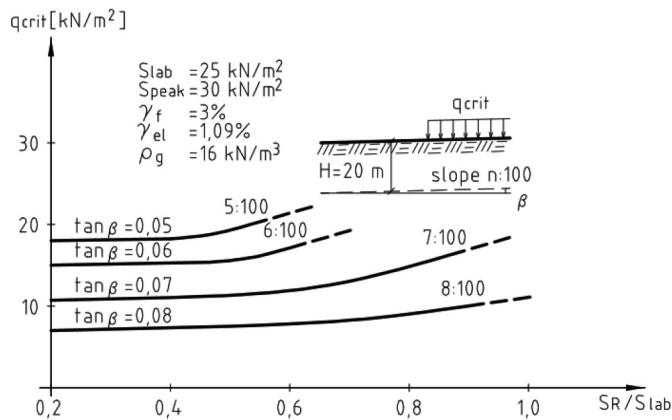
gradient. The diagram also accentuates the acute hazard in respect of progressive failure related to local upslope fills and embankments.

Some issues typical of landslides in sensitive deformation-softening soils are

- Progressive failure entails that long slopes, which under drained conditions may have remained stable for thousands of years, can be destabilized by more or less undrained deformation-softening response in the clay by seemingly insignificant "local" disturbing agents such as embankments, fills, pile-driving, vibration or blasting.
- Analysis of slope stability in long slopes based on short local slip surfaces (whether circular-shaped or plane) may yield highly erroneous results, simply because these modes of failure do not correspond to the actual failure mechanism (Bernander 2011; Jostad et al 2013). A serious consequence of this issue, in particular for road construction, is that earth fills designed to counteract the weight of road embankments often involve acute risk of a much more serious slide event than the one meant to be prevented by the supporting fill arrangement.
- Although quick clays involve particular risk in connection with landslide hazard, there are other factors that decisively contribute to progressive landslide formation and development. Such factors are e.g., the "rate" of applying the triggering additional load, clay sensitivity, and the "geometric features" of the slope as exemplified in Figs. 5 and 19. The importance of investigating the influence of creep on the stability of slopes is discussed by Pusch et al. (2016).
- The finite difference analysis used for assessing progressive failure formation explains how it actually can come about that slides in soft sensitive clays tend to spread so far — i.e., often several hundred metres — over horizontal (or slightly inclining ground), deforming the soil mass in passive failure down to great depths as in the Surte and Tuve slides.
- The finite difference analysis also predicts that the incipient failure zone with its shear band tends to be established "far beyond" the foot of a slope well before the possible subsequent collapse in passive failure which, in fact, may or may "not" actually occur.

Conclusions

The paper gives the following answer to the questions posed in the section titled "Introduction":

1. "Local additional load effects" may trigger extensive disastrous landslides in long natural slopes due to the sensitivity of the soil and to unfavorable slope features. In cases where the

triggering load is surprisingly small, there may be parts of the slope area where the resistant earth pressure just barely manages to carry the effects of gravitational forces.

2. The shear deformations in the "entire highly sheared zone" must be considered in the analysis to be able to properly study the states of equilibrium and deformations in a slope. The size of the triggering load is directly dependent on the possible deformations in this zone (in a very narrow shear band, the triggering load would be insignificant). Landslides in western Sweden indicate that this highly sheared zone may well extend over a third of the depth of the potentially sliding soil volume.
3. It is imperative to distinguish between "different phases" of a progressive landslide to understand the mechanisms of the slide and the different "time scales" in the different phases. Rates of loading as well as rates of change of shear stress are vital factors to be considered.
4. "A singular" case of static loading or a singular failure criterion is not sufficient to assess the stability of a long slope of sensitive clay. At least two critical conditions have to be analyzed based on the in situ conditions:
   (*a*) The "triggering" condition due to additional loading, (phase 2);
   (*b*) The "downslope passive failure" condition defining the minimum extent and the scope of landslide disaster, (phase 4).
   Dynamic forces may likely increase the final length of a landslide.
5. Zones of "unfractured clay" (stage I) and "deformation softening clay" in an established failure surface (stage II) must be treated separately as they have vastly different properties.
6. Failure zones and slip surfaces tend to develop far beyond the foot of a slope, i.e., even "prior" to the incidence of possible passive failure. This is due to the fact that the pressure required to generate a progressive failure along a plane — more or less parallel to the ground surface — may actually be much lower than the passive earth pressure resistance of the soil layers above this failure plane.

It should now be the time for consulting geotechnical engineers to start applying progressive failure analysis to long slopes with sensitive soils, especially if the triggering load is of local character. Yet, firstly, a basic understanding of the slide mechanisms is needed and the main purpose of this paper is to facilitate such an understanding. Secondly, a viable tool is needed for the analysis and as such, the FDM is outlined here. Finite element methods are also apt for this purpose.

Finally it should be added that more research is needed, in particular regarding the residual shear resistance of sensitive clays and its manifest dependence of loading rate, excess pore-water dissipation, in situ porosity of mixed sandy clay, and the degree of overconsolidation.

Acknowledgements

References

Aas, G., 1966. Special field vane tests for the investigation of shear strength of marine clays. Norwegian Geotechnical Institute, Oslo. Report 68. [In Norwegian.]

Bernander, S. 1978. Brittle failures in normally consolidated soils. Väg- & Vattenbyggaren (Stockholm), No. 8–9, pp. 49–52. [Most of Stig Bernander's publications are accessible at http://pure.ltu.se/portal/sv/publications/search.html.]

Bernander, S. 1985. On limit criteria for plastic failure in strain-rate softening soils. *In* Proceedings of the 11th ICSMFE, San Fransisco. Balkema. Vol. 1/A/2, pp. 397–400.

Bernander, S. 2000. Progressive landslides in long natural slopes. Formation, potential extension and configuration of finished slides in strain-softening soils. Licentiate thesis 2000:16, Luleå University of Technology. ISSN: 1402 – 1757. [Available at http://epubl.ltu.se/1402-1757/2000/16/index.html.]

Bernander, S. 2008. Down-hill progressive landslides in soft clays. Triggering disturbance agents. Slide prevention over horizontal or gently sloping ground. Sensitivity related to geometry. Research Report 2008:11, Luleå University of Technology. ISSN: 1402-1528. [Available at http://epubl.ltu.se/1402-1528/2008/11/index.html.]

Bernander, S. 2011. Progressive landslides in long natural slopes. Formation, potential extension and configuration of finished slides in strain-softening soils. Doctoral thesis, Luleå University of Technology, Division of Soil Mechanics and Foundation Engineering in cooperation with the Division of Structural Engineering, 3rd revised version, April 2012. ISBN 978-91-7439-283-8. [Available at http://pure.ltu.se/portal/files/36517492/Stig_Bernander.Rev._April_2012.pdf (accessed 26 November 2015).]

Bernander, S., and Gustås, H.K.G. 1984. Consideration of in situ stresses in clay slopes with special reference to progressive failure analysis. *In* Proceedings of the IVth International Symposium on Landslides, Toronto, Ont. Canadian Geotechnical Society. Vol. 2, pp. 235–240.

Bernander, S., and Olofsson, I. 1981. On formation of progressive failures in slopes. *In* Proceedings of the 10th International Conference on Soil Mechanics and Foundation Engineering, ICSMFE. Stockholm, 1981. Vol. 3, 11/6, pp. 357–362.

Bernander, S., Svensk, I., Holmberg, G., Bernander, J., and Isacsson, K. 1985. Shear strength and deformation properties of clays in direct shear tests at high strain rates. *In* Proceedings of the 11th ICSMFE, San Francisco. Balkema. Vol. 2/B/5, pp. 987–990.

Bernander, S., Gustås, H., and Olofsson, J. 1989. Improved model for progressive failure analysis of slope stability. *In* Proceedings of the 12th ICSMFE, Rio de Janeiro. Balkema. Vol. 21/3, pp. 1539–1542.

Bishop, A.W. 1971. The influence of progressive failure on the choice of the method of stability analysis. [Technical notes.] Géotechnique, **21**: 168–172. doi:10.1680/geot.1971.21.2.168.

Bjerrum, L. 1967. Progressive failure in slopes of over-consolidated plastic clay and shales. 3rd Terzaghi Lecture presented in Miami Florida 1966. Journal of the Soil Mechanics and Foundations Division, ASCE, **93**(5): 3–49.

Bonadies, F., Nordal, S., Gylland, A.S, Grimstad, G., Jostad, H.P., Cuomo, S., and Cascini, L. 2014. Numerical methods for simulation of downward progressive landslides. *In* Numerical methods in geotechnical engineering. *Edited by* M.A. Hicks, R.B.J. Brinkgreve, and A. Rohe. Taylor & Francis Group, London. pp. 579–584, ISBN 978-1-138-00146-6.

Caldenius, C., and Lundström, R. 1956. The landslide at Surte on the Göta River. Geological Survey of Sweden. SGU Report No. 27. Publ. Stockholm.

Chen, S.Y., Zhang, X.S., and Tang, W.S. 1997. A numerical method for analyzing progressive process of landslide in soil slope. *In* Proceedings of the 9th International Conference on Computer Methods in Geomechanics, Wuhan, China. Balkema. Vol. 13, pp. 1627–1642.

Christian, J.T., and Whitman, R.V. 1969. A one-dimensional model for progressive failure. *In* Proceedings of the 7th International Conference on Soil Mechanics and Foundation Engineering, Mexico City. Sociedad Mexicana de Mecanica de Sulelos. Vol. 2, pp. 541–545.

Flodin, N., and Broms, B. 1981. History of civil engineering in soft clay. *In* Soft clay engineering. *Edited by* E.W. Brand and R.P. Brenner. Elsevier, Amsterdam. pp. 25–156. ISBN 0-444-41784-2.

Graham, J., Crooks, J.H.A., and Bell, A.L. 1983. Time effects on the stress-strain behaviour of natural soft clays. Géotechnique, **33**(3): 327–340. doi:10.1680/geot.1983.33.3.327.

Gylland, A.S. 2012. Material and slope failure in sensitive clays. Doctoral thesis, Department of Civil and Transport Engineering, Norwegian University of Science and Technology, Trondheim. 2012:352.

Gylland, A.S., and Jostad, H.P. 2010. Effect of updated geometry in analysis of progressive failure. *In* Proceedings of the 7th European Conference on Numerical Methods in Geotechnical Engineering, Trondheim, Norway, 2–4 June 2010. *Edited by* T. Benz and S. Nordal. pp. 497–502.

Gylland, A.S., Jostad, H.P., and Nordal, S. 2014. Experimental study of strain localization in sensitive clays. Acta Geotechnica, **9**(2): 227–240. doi:10.1007/s11440-013-0217-8.

Jostad, H.P., Fornes, P., and Thakur, V. 2013. Effect of strain-softening in design of fills on gently inclined areas with soft sensitive clays. *In* Landslides in sensitive clays. From geoscience to risk management. *Edited by* J.-S. L'Heureux, A. Locat, S. Leroueil, D. Demers, and J. Locat. Springer. pp. 305–316. ISBN 978-94-007-7078-2.

Kjellman, W. 1955. Mechanics of large Swedish landslides. Géotechnique, **5**(1): 74–78. doi:10.1680/geot.1955.5.1.74.

L'Heureux, J.-S., Locat, A., Leroueil, S., Demers, D., and Locat, J. (*Editors*). 2013. Landslides in sensitive clays. From geoscience to risk management. Springer. ISBN 978-94-007-7078-2.

Larsson, R., and Jansson, M. 1982. The landslide at Tuve, November 30, 1977. Swedish Geotechnical Institute, Linköping. Report No 18.

Leroueil, S. 2001. Natural slopes and cuts: movement and failure mechanisms.

39th Rankine Lecture. Géotechnique, **51**(3): 197–243. doi:10.1680/geot.51.3.197.39365.

Locat, A. 2007. Ètude d'un étalement latéral dans les argiles de l'est du Canada et de la rupture progressive. Le cas du glissement de Saint-Barnabé-Nord. M.Sc. thesis, Departement de Génie Civil, Faculté de Sciences et de Genie, Université Laval, Quebec City, Que.

Locat, A. 2012. Rupture progressive et étalements dans les argiles sensibles. [Progressive failure and spreads in sensitive clays.] Ph.D. thesis, Département de génie civil et de génie des eaux, Université Laval, Quebec City, Que.

Locat, A., Leroueil, S., Bernander, S., Demers, D., Locat, J., and Ouehb, L. 2008. Study of a lateral spread failure in an eastern Canada clay deposit in relation with progressive failure: The Saint-Barnabé-Nord Slide. *In* Proceedings of the 4th Canadian Conference on Geohazards. From Causes to Management. *Edited by* J. Locat, D. Perret, D. Turmel, D. Demers, and S. Leroueil. Presses de l'Université Laval, Quebec City, Que. pp. 89–96.

Locat, A., Leroueil, S., Bernander, S., Demers, D., Jostad, H.P., and Ouehb, L. 2011. Progressive failures in eastern Canadian and Scandinavian sensitive clays. Canadian Geotechnical Journal, **48**(11): 1696–1712. doi:10.1139/t11-059.

Locat, A., Jostad, H.P., and Leroueil, S. 2013. Numerical modeling of progressive failure and its implications for spreads in sensitive clays. Canadian Geotechnical Journal, **50**(9): 961–978. doi:10.1139/cgj-2012-0390.

Locat, A., Leroueil, S., Fortin, A., Demers, D., and Jostad, H.P. 2015. The 1994 landslide at Sainte-Monique, Quebec: geotechnical investigation and application of progressive failure analysis. Canadian Geotechnical Journal, **52**(4): 490–504. doi:10.1139/cgj-2013-0344.

Löfquist, B. 1973. Lerskred genom vattenupptryck. [Slides in clays caused by hydraulic uplift.] Väg- och vattenbyggaren, Stockholm, **19**(2): 187–190. [In Swedish.]

Pusch, R., Knutsson, S., Liu, X., and Yang, T. 2016. Creep can strengthen clay: a matter of long-term slope stability. Journal of Earth Sciences and Geotechnical Engineering, **6**(1): 1–18. Scienpress Ltd. ISSN: 1792-9040 (print), 1792-9660 (online).

Puzrin, A.M. 2016. Editorial: Modern trends in landslide mechanics. Géotechnique, **66**(3): 173–174. doi:10.1680/jgeot.2016.66.3.173.

Quinn, P. 2009. Large landslides in sensitive clay in eastern Canada and the associated hazard risk to linear infrastructure. Ph.D. thesis, Department of Geological Sciences and Geological Engineering, Queen's University, Kingston, Ont. Available at: http://qspace.library.queensu.ca/handle/1974/1781 [accessed 21 April 2011].

Rehnström, L. 2013. Analysis of progressive landslides. A review of the simplified calculation model. M.Sc. thesis, Division of Geo Engineering, Chalmers University of Technology, Göteborg, 2013:5. Available at http://publications.lib.chalmers.se/records/fulltext/185611/185611.pdf.

Saurer, E. 2009. Shear band propagation in soil and dynamics of tsunamigenic landslides. Ph.D. thesis, ETH, Zürich. doi:10.3929/ethz-a-005951122. Available at http//www.civil.iitb.ac.in/e.library.queensu.

Skempton, A.W. 1964. Fourth Rankine Lecture: Long term stability of clay slopes. Géotechnique, **14**(2): 77–102. doi:10.1680/geot.1964.14.2.77.

Terzaghi, K., and Peck, R.B. 1948. Soil mechanics in engineering practice. New York, John Wiley & Sons, Inc.

Thakur, V. 2007. Strain localization in sensitive soft clays. Ph.D. thesis, Geotechnical Division, Department of Civil and Transport Engineering, Norwegian Institute of Science and Technology, NTNU. International Centre for Geohazards, Trondheim and Norwegian Centre of Excellence. ISBN 9788247139097.

Thakur, V., and Septanika, E.G. 2008. Extended finite element modeling (X-FEM) of progressive sliding in geomaterials, In Proceedings of the Nordic Geotechnical Meeting, No. 15. *Edited by* K. Flaate, T.-E. Frydenlund, J. Prestegarden, and K. Senneset. pp. 447–469.

Troncone, A. 2005. Numerical analysis of a landslide in soils with strain-softening behaviour. Géotechnique, **55**(8): 585–596. doi:10.1680/geot.2005.55.8.585.

Zabala, F., and Alonso, E.E. 2011. Progressive failure of Aznalcollar dam using the material point method. Géotechnique, **61**(9): 795–808. doi:10.1680/geot.9.P.134.

Zhang, W., Wang, D., Randolph, M.F., and Puzrin, A.M. 2015. Catastrophic failure in planar landslides with a fully softened weak zone. Géotechnique, **65**(9): 755–769. doi:10.1680/geot14.P.218.

List of symbols

E — total downslope earth pressure ($= E_o + N$); or the modulus of elasticity

F — safety factor at failure conditions

G — shear modulus

H — depth of a failure plane under the ground surface

K — relationship between horizontal and vertical stresses (in general the total stress)

L — length of the failure zone

N — downhill compression force acting above the assumed potential (or the established) failure surface due to the triggering load

q — locally applied triggering surface load

s — peak shear stress ($= \tau_{max}$)

t time

x coordinate along the potential or the established failure plane, where $x = 0$ defines a point where the influence of N_q is negligible

z vertical coordinate from the failure plane

α relative thickness of the zone where the shear deformation takes place

β inclination of a studied slope or of a part of the same

γ shear deformation

δ deformation caused by compression shear forces, slip; or a differential part of a function

ν Poisson's ratio

ρg density where g is the gravitational acceleration

σ normal stress

τ shear stress

Indices

o   denotes in situ parameters

a, b, c, d, e   different moments during a slope failure

crit   critical value

el   elastic

f   failure; or value at maximum

h   horizontal

I   failure condition 1 (in eq. (1))

II   failure condition 2 (in eq. (2))

instab   value when a parameter changes from a stable to an unstable condition

L   length of failure zone

l, lab   laboratory

max   maximum

mean   mean value

N   downhill compressive force

P   passive earth pressure

p   length of passive Rankine failure zone at the end of the slope

q   caused by a load q

R   residual

Rankine   Rankine earth pressure condition

s   safety

slip   inelastic slip displacement

v   vertical

Appendix A. Basic procedure using the finite difference method

Figure A1 illustrates the principles and the integration procedure for the proposed FDM of analysis. The aim is to determine the maximum load effect, q_{crit}, that can be applied in a certain upslope location.

The integral computation begins at a point, $x = 0$, further down the slope, where the conditions of stress and deformation are unaffected by the applied additional load, N_q. Hence, the parameters for earth pressure $E_{0,x=0}$, in situ shear stress $\tau_{0,x=0}$, load effect $N_{x=0}$ and downslope displacement $\delta_{x=0}$ constitute the downslope boundary condition for the subsequent integral analysis. Correspondingly, the force N_L at $x = L$ is the upslope boundary condition that, when satisfied, determines the associated values of $\tau_{x=L}$ and $\delta_{x=L}$. The force $N_L = f(q)$ can often here approximately be taken as $N_L \approx qH_L$, where q(kN/m²) is the applied load and H_L(m) is the height of the slope. In Fig. A1, the boundary condition at $x = 0$ is defined as: $E_x = E_{0,x=0}$, $\tau_x = \tau_{0,x=0}$, $N_x = 0$, and $\delta_x = 0$. The procedure can be subdivided into the following steps.

Step 1

The integration process starts at a point ($x = 0$) further down the slope, where the influence of the additional load N_q is negligible, by choosing an initial shear stress increment at the potential failure plane $\Delta\tau_1$ at a distance $x = \Delta x_1$. The corresponding increase of the normal force N_1 and the associated downhill axial displacement δ_1 may then directly be determined, rendering the following values at x_1 namely τ_x, ($z = 0$) $= \tau_o + \Delta\tau_1 = \tau_1$, $N_x = N_1$ and $\delta_x(N_1) = \delta_1$.

Step 2

As indicated in Fig. A1, the calculation proceeds by advancing in steps of suitably chosen values of $\Delta\tau$ and Δx. As the values of δ_N and δ_τ can then be expressed in terms of the assumed values of the increments $\Delta\tau$ and Δx, the correlating values of Δx and $\Delta\tau$ in each step cycle have to be found by iteration so that the compatibility equation is satisfied, i.e.:

$$\delta_{N,x} = \sum\nolimits_0^x (\Delta\delta_N) = \delta_{\tau,x}$$

A trial value for $\Delta\tau_2$ and a corresponding value of $x_2 = x_1 + \Delta x_2$ are assumed. The value of N_2 is then $N_1 + \Delta\tau\Delta x_2$ and the related value of additional displacement $\Delta\delta_x(N_{1-2}) = (N_1 + N_2)\Delta x_2/(2HE_{clay})$ and $\delta_x(N_2) = \delta_2$ can be calculated. Here E is the compression modulus of elasticity of the clay. Yet, the downhill displacement $\delta_x(N_2)$ has to be compatible with the shear deformation $\delta_x(\tau_2)$ at x_2. This value is determined by integration over the zone subject to intense shear – i.e., from $z_{x,2} = 0$ to $z_{x,2} = \alpha H_x$, where α is a measure of the thickness of this zone, (α usually taken to be about one-third in accordance with data from studies of landslides occurred of the current kind). The shear zone is subdivided into differentials of Δz.

However, the double integration analysis being an iterative procedure, a compatibility criterion demanding that $\delta_x(N_2) = \delta_x(\tau_2)$ has to be satisfied. This condition is not likely to be fulfilled in the first attempt, i.e., $\delta_x(\tau_2) \neq \delta_x(N_2)$.

By selecting new values of $\Delta\tau$, this equation can readily be adjusted so that the compatibility criterion is satisfied, i.e.,

$$\delta_x(\tau) = \delta_x(N)$$

Step 3

At this point, a new stress increment $\Delta\tau_3$ at $x_3 = x_2 + \Delta x_3$ is tried, again determining the corresponding increase of the normal force N_3 and the downhill displacement $\delta_3(N)$.

In each step of the continued integration process, the downhill displacement is determined by repeating the iterative procedure in step 2, whereby also the parameters $\tau_{x,z=o}$, N_x, and δ_x are calculated for each value of x. The boundary condition to be satisfied in the current case is that N_x for $x = L$ is equal to the additional load $N_q \approx qH_L$. In slopes with complex geometry, this boundary condition is not initially likely to be fulfilled, in which case an alternative position for the starting point ($x = 0$) has to be chosen.

This analysis may appear to be extremely laborious. Yet, using computer software, a trial and error integration of this kind is a matter of seconds once all relevant slope data have been introduced. Applications using spreadsheets are given in Appendices in Bernander (2008, 2011). The spreadsheet has also been used by, e.g., Locat (2007) and in a simplified version by Rehnström (2013).

Fig. A1. Section illustrating calculation procedure.